ELSEVIER

Journal of Alloys and Compounds 356–357 (2003) 730–733

Journal of ALLOYS AND COMPOUNDS

www.elsevier.com/locate/jallcom

Influence of polymorphism on the electrochemical properties of $(Ti_{0.64}Zr_{0.36})Ni$ alloys

F. Cuevas[a,*], M. Latroche[a], P. Ochin[b], A. Dezellus[b], A. Percheron-Guégan[a]

[a] *LCMTR-ISCSA-CNRS, 2–8 Rue Henri Dunant, 94320 Thiais Cedex, France*
[b] *CECM-ISCSA-CNRS, 15 Rue Georges Urbain, 94407 Vitry sur Seine, France*

Received 5 July 2002; accepted 15 November 2002

Abstract

Key electrochemical properties of austenitic and martensitic $(Ti_{0.64}Zr_{0.36})Ni$ alloys as regards their use as negative electrodes for Ni–MH batteries have been studied. Austenitic alloys exhibit a reversible capacity of 85 mAh/g, at a discharging rate of C/10, without notable capacity decay upon electrochemical cycling. In contrast, martensitic alloys possess, at the same regime, a much higher reversible capacity, 330 mAh/g, though a shorter cycle-life. These dissimilar results are due to the remarkable thermodynamic differences for hydrogen absorption between both structures. Besides, it has been observed that both phases neither decompose nor suffer any phase transformation upon repeated hydrogen absorption/desorption cycling. Capacity decay in martensite seems to be associated to surface passivation effects which are favoured by mechanical decrepitation.
© 2003 Elsevier B.V. All rights reserved.

Keywords: Electrode materials; Intermetallics; Crystal structure

1. Introduction

The TiNi alloy exhibits polymorphism. On cooling, it undergoes a martensitic transformation near room temperature from a cubic CsCl-type structure (denoted as austenite) to a monoclinic TiNi-type structure (martensite). This transformation is the basis of its shape memory behaviour [1]. The transformation temperature depends on the alloy composition and, moreover, on the mechanical and thermal history of the alloy, i.e. on its microstructure. By using different cooling rates during alloy preparation, either martensitic or austenitic structures can be obtained for a given temperature and composition, as has been recently reported for $(Ti_{1-y}Zr_y)Ni$ alloys with $0 \leq y < 0.5$ [2].

So, early as 1970, Justi et al. noticed the outstanding properties of the AB-type TiNi alloy as a reversible negative electrode for Ni–MH batteries [3]. The TiNi alloy has a rather low specific weight, good oxidation resistance and notable hydrogen reversible capacity: 245 mAh/g [3,4] from electrochemical discharge measurements. As a main drawback, discharge kinetics are slow despite its high electrocatalytic activity for the hydrogen electrode reaction [5,6]. Unfortunately, little attention has been paid in the literature to establish to which crystal structure correspond the reported hydrogenation properties of the TiNi alloy. In this paper, we report on the reversible electrochemical capacity and cycle-life of martensitic and austenitic structures in the Zr-substituted $(Ti_{0.64}Zr_{0.36})Ni$ alloy.

2. Experimental

AB-type alloys with nominal composition $(Ti_{0.64}Zr_{0.36})Ni$ having either martensitic or austenitic structures were prepared as discussed in a previous publication [2]. Their hydrogen absorption/desorption pressure–composition (P–C) isotherms were obtained at 403 K within the pressure range 0.1–20 bar by using the volumetric method. Distinct austenitic and martensitic powder electrodes were prepared as now described. As TiNi-type intermetallic compounds are extremely tough to fracture, both martensitic and austenitic alloys were hydrogenated by gas–solid reaction to obtain them in a powder state. Hydrogenation was conducted at 373 K and hydrogen pressure of 10 bar. This treatment only weakens the austenite, whereas it pulverizes the martensite. After cooling at room temperature, hydrogen content in the

*Corresponding author.
E-mail address: fermin.cuevas@glvt-cnrs.fr (F. Cuevas).

0925-8388/03/$ – see front matter © 2003 Elsevier B.V. All rights reserved.
doi:10.1016/S0925-8388(03)00081-1

alloys are $x=1.6$ for the austenite and $x=2.8$ for the martensite (where x denotes hydrogen-to-formula unit atomic ratio: H/AB). Such hydrides were mechanically crushed, sieved under 100 μm and mixed with conductive carbon and polytetrafluoroethylene (PTFE) in the weight ratio 90:5:5. These composites were rolled to obtain sheets of 250 μm thickness. Finally, austenitic and martensitic hydride electrodes were produced by cold-pressing at 245 MPa of the respective composite on a nickel grid.

Electrochemical experiments were accomplished in a one-compartment cell which comprises the negative working-electrode, an $Ni(OH)_2$/NiOOH counter-electrode, an Hg/HgO reference electrode and 7.8 M KOH as electrolyte. Electrode discharge capacity was determined by the galvanostatic method using a MacPile device from Biologic. A common current density of 0.03 A/g was used for both kind of electrodes, which roughly corresponds to a regime of C/10. The cut-off potential was fixed at −0.7 V vs. Hg/HgO. Structural and morphological state of the electrodes after cycling were studied by X-ray diffraction (XRD) using Cu Kα radiation in a Bruker AXS D8Advance θ–θ diffractometer and by scanning electron microscopy (SEM).

3. Results and discussion

P–C isotherm curves for austenite and martensite are displayed in Fig. 1. Hydrogen enters topotactically, i.e. as a solid solution, in the austenitic alloy exhibiting neither plateau pressure nor hysteresis effects. This result agrees with previous solid–gas [7] and electrochemical [8] measurements in cubic-TiNi alloys. On the contrary, hydrogen absorption/desorption in martensite occurs through a two-phase coexistence region which extends from $x=1.0$ to $x=2.1$ and displays a strong hysteresis behaviour. At a hydrogen pressure of 10 bar, the storage capacity of the austenitic phase only attains $x=1.5$, whereas it reaches as much as $x=2.5$ for martensite. Strikingly, hydride formation in martensite-TiNi resembles that of the ZrNi alloy, not only in thermodynamic terms [9] but also in mechanical stability. Full hydride formation in martensite-TiNi and ZrNi causes alloy pulverisation [10].

The electrochemical reversible capacity for both austenitic and martensitic structures as a function of cycle-number is shown in Fig. 2. Both electrodes reach their maximum capacity, C_{MAX}, after an activation period of about 10 cycles. Since electrodes initially consist of hydride powders, the activation stage is attributed to the reduction of an oxide surface layer and not to hydrogen-induced bulk changes. This layer has been already reported to occur in Ti–Zr–Ni electrodes [11] and is likely formed during electrode preparation under atmospheric conditions.

C_{MAX} reaches 85 mAh/g for the austenite and 329 mAh/g for the martensite, i.e. $\Delta x_{MAX}=0.39$ and 1.50, respectively, according to the equation:

$$\Delta x_{MAX} = \frac{3.6W}{F} \cdot C_{MAX} \ (\text{mAh/g}) \quad (1)$$

where W is the molecular weight of the alloy and F is the Faraday constant. Δx_{MAX} for both structures roughly corresponds to the hydrogen stored within two decades of pressure in solid–gas process, respectively (Fig. 1). The TiNi alloy was reported to have a reversible capacity of 245 mAh/g ($\Delta x \sim 1.1$) when very slow discharge rates are used [3,4]. We can ascribe those results as belonging to the austenite. A much higher reversible capacity is obtained for the martensite, in agreement with its *P–C* isotherm curves, even at quite fast discharging rates, C/10. It is worth noting that martensite C_{MAX} is comparable to that of $LaNi_5$-type alloys [12].

Cycle-life behaviour of austenitic and martensitic electrodes differs considerably. In comparison with their respective C_{MAX} values, the capacity decay for the austenite is of 18% after 113 cycles, whereas it reaches for the

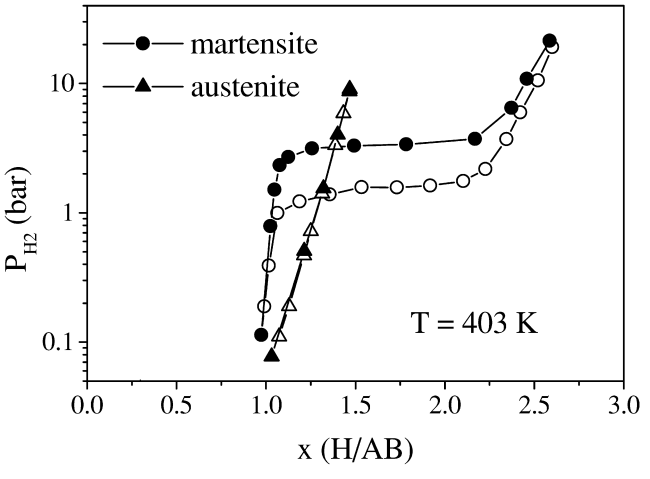

Fig. 1. *P–C* isotherm curves at 403 K of martensitic and austenitic $(Ti_{0.64}Zr_{0.36})Ni$ alloys. Full symbols correspond to absorption and empty symbols to desorption.

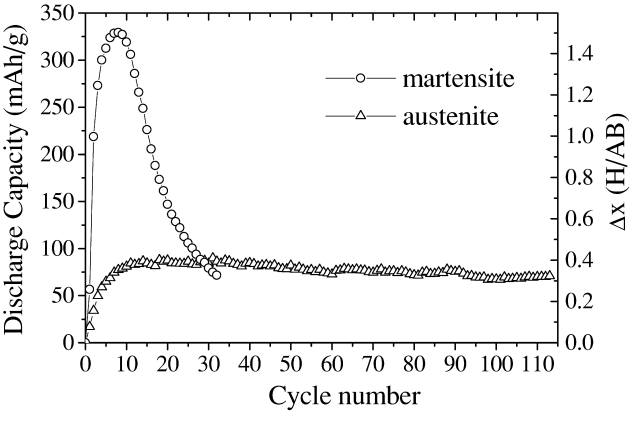

Fig. 2. Reversible discharge capacity of martensitic and austenitic alloy electrodes as a function of cycle number.

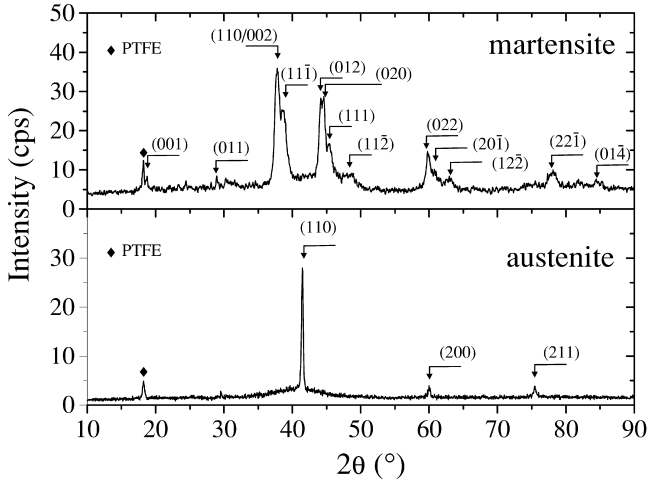

Fig. 3. XRD patterns of martensitic (top) and austenitic (bottom) electrodes after 32 and 113 electrochemical cycles, respectively. Peak reflections are indexed according to the monoclinic $P2_1/m$ and cubic $Pm\bar{3}m$ space groups for martensitic and austenitic electrodes, respectively.

martensite as much as 76% after only 32 cycles. XRD patterns of both electrodes after such cycling treatments are shown in Fig. 3. Except for an extra peak at $2\theta = 18.2°$, which matches with the strongest intensity line of PTFE [13], both patterns are fully indexed to their respective original alloy structures. Therefore, no martensitic phase transformation takes place upon cycling and, moreover, no new crystalline phases such as metallic oxides or hydroxides are formed during electrolytic experiments at quantities higher than the XRD detection level (typically ~5% in weight). Cycled-austenite has a CsCl-type structure with cell parameter $a = 3.088(1)$ Å and cell volume 29.46(2) Å^3/AB. Cycled-martensite is monoclinic (space group $P2_1/m$) with cell parameters $a = 3.066(3)$ Å, $b = 4.082(4)$ Å, $c = 4.920(4)$ Å, $\beta = 104.02(3)°$ and cell volume 29.87(5) Å^3/AB. These cell volumes are similar to those of hydrogen-free $(Ti_{0.64}Zr_{0.36})Ni$ alloys [2]. Spontaneous hydrogen desorption is thought to be caused by catalytic effects when electrodes are exposed to the air, in agreement with previous observations for the TiNi alloy [14].

The morphological changes of the alloy particles after electrochemical cycling can be observed in the SEM results shown in Fig. 4. The austenite exhibits a well-defined geometry without notable changes on cycling. In contrast, the martensite has a much more complex surface morphology. This feature is already observed before electrochemical cycling and is attributed to spontaneous cracking during solid–gas reaction pre-treatment. Upon electrochemical cycling, martensitic grains suffer additional bulk decrepitation. Such different behaviour between martensitic and austenitic electrodes is directly related to their different P–C isotherm curves (Fig. 1). Hydrogen absorption/desorption in martensite occurs through a two-phase domain region that involves two hydride phases with distinct cell volumes. While accomplishing this phase transformation, the mechanical stresses developed at the interface between both hydride phases induce decrepitation. This mechanism has been already invoked to explain mechanical instability in $LaNi_5$-type alloys [15]. On the other hand, topotactic H-insertion in austenite does not cause severe grain cracking as no phase transformation takes place.

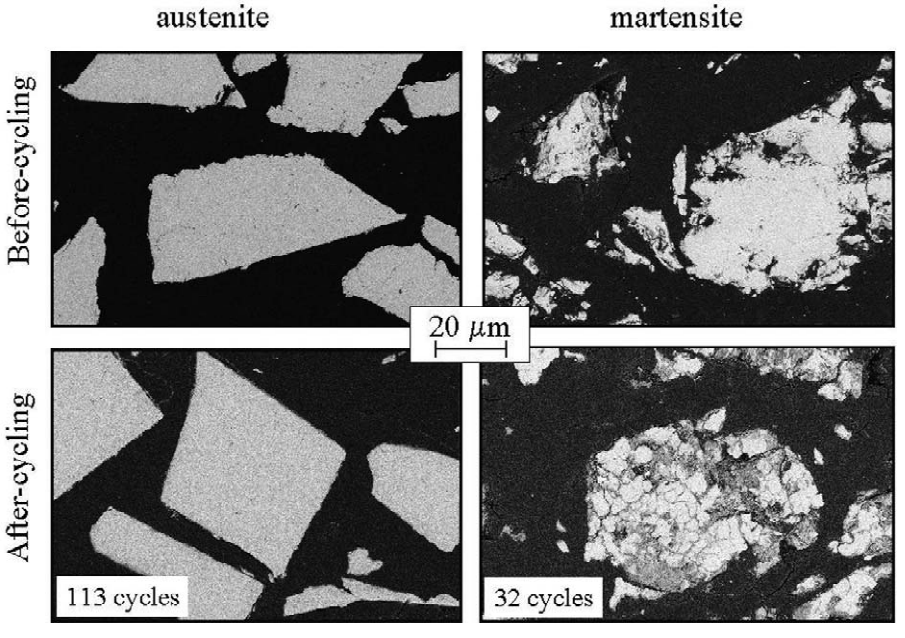

Fig. 4. Backscattered electron micrographs, obtained by SEM at 5 kV, of austenitic (left) and martensitic (right) electrodes before (up) and after (down) electrochemical cycling.

In $LaNi_5$-type alloys, the capacity decrease is attributed to the decomposition of the alloy and to the formation of metallic hydroxides, i.e. to the loss of active mass [12,15]. This seems not to be the case for martensitic (Ti,Zr)Ni alloy as no new phases are observed by XRD after cycling. Furthermore, SEM observations of the cycled-martensitic electrode (Fig. 4, right–bottom) do not show extended corroded alloy regions compatible with the strong capacity decay (76%). These facts point, however, towards a surface passivation effect as reported for Ti–Zr–V–Mn–Ni AB_2-type alloys [16]. Thus, the growth of superficial oxide or hydroxide layers (not thick enough to be detected by XRD) during electrochemical cycling hinders hydrogen transfer at the grain surface. In fact, energy dispersive X-ray analysis coupled at the SEM device has revealed important oxygen contents in grain cracks (gray areas in Fig. 4, right–botton). This may also indicate that decrepitation favours surface passivation, which, in turn, agrees with the long cycle-life of austenitic electrodes. The composition of the electrolytic passivation layer must be different to the atmospheric one responsible of the initial activation stage. Precise characterisation of both passivation layers requires further analysis by nanoscale-resolved microscopy techniques or surface sensitive electrochemical measurements.

Acknowledgements

The authors wish to thank F. Briaucourt and E. Leroy for technical assistance and J.-L. Pastol for SEM observations.

References

[1] K. Otsuka, X. Ren, Intermetallics 7 (1999) 511.
[2] F. Cuevas, M. Latroche, P. Ochin, A. Dezellus, J.F. Fernández, C. Sánchez, A. Percheron-Guégan, J. Alloys Comp. 330–332 (2002) 250.
[3] E.W. Justi, H.H. Ewe, A.W. Kalberlah, N.M. Saridakis, M.H. Schaefer, Energy Convers. 10 (1970) 183.
[4] M.A. Gutjahr, Ph.D. Thesis, Geneva University, Geneva, 1974.
[5] M.H. Miles, Electroanal. Chem. Interfacial Electrochem. 60 (1975) 89.
[6] K. Machida, M. Enyo, G. Adachi, J. Shiokawa, Electrochim. Acta 29 (1984) 807.
[7] R. Burch, N.B. Mason, J. Chem. Soc., Faraday Trans. I 75 (1979) 561.
[8] M. Schreiber, R.A. Huggins, K. Maly, Solid State Ionics 28–30 (1988) 873.
[9] W. Luo, A. Craft, T. Kuji, H.S. Chung, T.B. Flanagan, J. Less-Common Met. 162 (1990) 251.
[10] N. Michel, S. Poulat, L. Priester, P. Dantzer, M. Gupta, J. Phys. IV France 12 (2002) Pr2–183.
[11] S. Wakao, Y. Yonemura, H. Nakano, H. Shimada, J. Less-Common Met. 104 (1984) 365.
[12] F. Cuevas, M. Latroche, J.-M. Joubert, A. Percheron-Guégan, Appl. Phys. A 72 (2001) 225.
[13] X-Ray Powder Diffraction File No. 47-2217 for Polytetrafluoroethylene PTFE, JCPDS-ICDD, International Center for Diffraction Data, Pennsylvania, USA, 1995.
[14] D.-Y. Yan, J. Alloys Comp. 209 (1994) 257.
[15] J.J.G. Willems, Philips J. Res. Suppl. 39 (1984) 1.
[16] H.-H. Lee, K.-Y. Lee, J.-Y. Lee, J. Alloys Comp. 253–254 (1997) 601.